Improving Gyroscope's Noise Performance By Embedding it in a Closed-Loop Involving Multiple Accelerometers

Dimitris Nikitas*, Konstantinos Papafotis† and Paul P. Sotiriadis‡
Department of Electrical and Computer Engineering
National Technical University of Athens, Greece
Email: *dimitrisnkts@gmail.com †k.papafotis@gmail.com, ‡pps@ieee.org

***Abstract*—This work introduces an inertial measurement unit (IMU) architecture which combines several three-axis accelerometers and a three-axes gyroscope to provide an increased accuracy, low-noise measurement of the angular velocity. This is an extension of gyroscope-free IMUs, which use only accelerometers to measure the linear acceleration and translate it to angular velocity by solving a system of differential equations. Existing architectures cannot compensate for the accelerometers' bias which integrated is translated to a constant drift of angular velocity. The proposed system exploits the basic operating principles of the gyroscope-free IMUs and uses a three-axis gyroscope in a closed-loop configuration to compensate for the effect of the accelerometers' bias. Focusing on a very popular and highly cited IMU, the stability of the proposed system is proved analytically. Simulation results indicate that the proposed architecture excels in terms of noise performance; in the upper frequency range, it presents up to 30dB less noise at its output compared to the gyroscope.**

***Index Terms*—Accelerometer, gyroscope, inertial measurement unit, IMU, low-noise**

I. Introduction

INERTIAL sensors (accelerometers and gyroscopes) are nowadays embedded in several commercial devices such as smartphones, activity trackers, alarm systems and others while they are also used in many high-end, industrial, marine, aerospace and military applications. The fast development of Micro-Elctro-Mechanical (MEM) inertial sensors over the past decades enabled the wider use of inertial sensors. Their miniature size and extremely low cost make MEM inertial sensors the ideal choice for a plethora of applications. However, their large error characteristics and measurement noise [1] forbid their use in applications where measurement accuracy is important.

The measurement errors sourcing from manufacturing imperfections are (in their greatest part) static and there are several calibration techniques that can effectively compensate for them [2], [3].

The non-deterministic measurement noise on the other hand is a more complicated problem which is most commonly dealt with using extra sensors or estimation and filtering techniques according to the specific application's specifications and needs. In inertial navigation for example, where the gyroscope's noise is causing a significant attitude error [4], it is common to use a Kalman filter [1], [5] or use additional sensors, such as a magnetometer [1], [6], to get a more accurate attitude estimation.

In this work we introduce an inertial measurement unit architecture which combines several three-axis accelerometers and a single three-axis gyroscope, in a closed-loop configuration, to effectively reduce the measurement noise of the angular velocity. The proposed architecture expands the basic operating principles of the gyroscope-free inertial measurement systems which use the measurements of several single-axis accelerometers alone to derive both the acceleration and the angular velocity. It uses several three-axis accelerometers, placed on a rigid object, in combination with a single three-axis gyroscope to alleviate the drift problems of the gyroscope-free inertial measurement systems (see Section II). The proposed architecture excels in terms of noise performance as, in the upper frequency range, it presents up to 30dB less noise at its output compared to the gyroscope.

II. Gyroscope-Free Inertial Measurement Systems

In this Section, the basic principle of operation of gyroscope-free inertial measurement systems is introduced. Then, a popular and highly cited architecture is presented and its performance limitations are highlighted.

A. Principle of Operation

Consider N single-axis accelerometers, placed arbitrary positions, $r_i, i = 1, 2, \ldots, N$ on a rigid body and denote their sensitivity axes and measurements as $\hat{\eta}_i$ and f_i, respectively. Following [7], we write the following system of equations for deriving the specific force (f) and the angular velocity (ω)

$$F = Jx + P \tag{1}$$

where

$$x = \begin{bmatrix} \dot{\omega} \\ f \end{bmatrix}, \quad J = \begin{bmatrix} J_1^T & J_2^T \end{bmatrix}$$
$$F = \begin{bmatrix} f_1 \\ f_2 \\ \vdots \\ f_N \end{bmatrix}, \quad P = \begin{bmatrix} \hat{\eta_1}^T \Omega^2 r_1 \\ \hat{\eta_2}^T \Omega^2 r_2 \\ \vdots \\ \hat{\eta_N}^T \Omega^2 r_N \end{bmatrix} \tag{2}$$

the auxiliary variables J_1 and J_2 are

$$\begin{aligned} J_1 &= \begin{bmatrix}(r_1 \times \hat{\eta_1}) & (r_2 \times \hat{\eta_2}) & \dots & (r_N \times \hat{\eta_N})\end{bmatrix} \\ J_2 &= \begin{bmatrix}\hat{\eta_1} & \hat{\eta_2} & \dots & \hat{\eta_N}\end{bmatrix} \end{aligned} \tag{3}$$

and Ω is the cross-product matrix of the vector $\omega \triangleq \begin{bmatrix}\omega_x & \omega_y & \omega_z\end{bmatrix}^T$

$$\Omega = \begin{bmatrix} 0 & -\omega_z & \omega_y \\ \omega_z & 0 & -\omega_x \\ -\omega_y & \omega_x & 0 \end{bmatrix} \tag{4}$$

Given an adequate number of properly placed (single-axis) accelerometers, one can solve (1) in a least squares sense and derive x as

$$x = \left(J^T J\right)^{-1} J^T (F - P) \tag{5}$$

Further defining $\bar{J} = \left(J^T J\right)^{-1} J^T$, (5) is written in a compact form as

$$x = \bar{J}F - \bar{J}P \tag{6}$$

and the solution is only valid if $J^T J$ is non-singular.

In this work, we focus on the solution of the system of differential equations for deriving the angular velocity, ω. Denoting the i^{th} row of $\bar{J}$ as $\bar{J}_i$, we write

$$\dot{\omega} = \hat{J}F - \hat{J}P \tag{7}$$

where

$$\hat{J} = \begin{bmatrix}\bar{J}_1^T & \bar{J}_2^T & \bar{J}_3^T\end{bmatrix}^T \tag{8}$$

B. Existing Art and Performance Limitations

Several gyroscope-free inertial measurement systems' architectures have been proposed over the years. Many authors have proposed architectures using six [7], nine [8]–[10], ten [11] or twelve [12], [13] (single-axis) accelerometers in an effort to provide a feasible solution to (7) and moreover simplify the original non-linear problem for estimating the angular velocity.

To demonstrate the performance limitations of the existing approaches using multiple accelerometers in open-loop configuration, we consider the most popular one, the cube-type IMU proposed by J. Chen [7] and further studied by several other authors [14]–[19]. Although we focus on only one architecture, our results can easily expanded to all existing architectures which use specific geometries for the sensors' placement in order to reduce the non-linear system of differential equations to a linear one.

The authors of [7] use just six single-axis accelerometers placed on the faces of a cube as shown in Figure 1. By doing so, the non-linear terms of (7) are eliminated and the derivative of the angular velocity is derived as a linear combination of the six accelerometers' measurements as follows

$$\dot{\omega} = \frac{1}{2l^2} J_1 F \tag{9}$$

While [7] provide a very simple and computationally light solution to the original non-linear problem, the analysis is limited to the case of ideal accelerometers and neglects the effects of noise, bias and other imperfections of a real-world accelerometer. Since the bias is the largest contributor in the accelerometer's measurement error [2], we will examine the effect of a small additive bias, δF on the accelerometer's measurements. In this case, (9) becomes

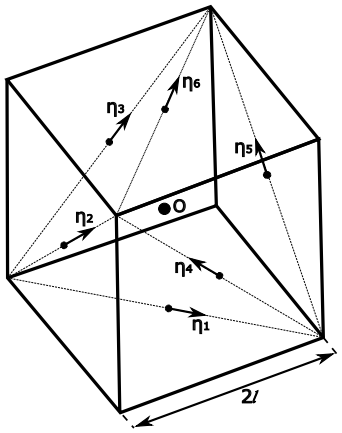

Fig. 1: Gyroscope-free inertial measurement system proposed in [7]. Six single-axis accelerometers are placed on the faces of a cube. Their sensitivity axes are denoted by $\hat{\eta_1}, \hat{\eta_2}, \dots, \hat{\eta_6}$.

$$\dot{\tilde{\omega}} = \frac{1}{2l^2} J_1 (F + \delta F) \tag{10}$$

where δF is the 6×1 vectors representing the accelerometers' bias. Subtracting (9) from (10) we get the evolution of the system's output error in time

$$\dot{\delta\omega} \triangleq \dot{\omega} - \dot{\tilde{\omega}} = \frac{1}{2l^2} J_1 \delta F \tag{11}$$

As seen in (11), the output error of the cube-type IMU accumulates over time meaning that even a very small offset in the accelerometers' measurements causes a cumulative angular velocity error. This is rather important as even if the static sensors' offset is removed by a calibration procedure, a small offset drift is expected over time, especially in the case of low-cost sensors.

III. The Proposed System

In this Section, the proposed inertial measurement system is introduced and analyzed in detail. The stability of the proposed system under the effects of the accelerometers' and gyroscope's biases is investigated. Simulations demonstrate the improved noise performance of the proposed system compared to a gyroscope of the same grade.

A. System Analysis

To alleviate the performance limitations of existing architectures, presented in Section II-B, the proposed system uses a three-axis gyroscope, placed at the center of the cube (point O in Figure 1). The top-level architecture of the proposed system is shown in Figure 2a and its block diagram representation is shown in Figure 2b.

Intuitively, the feedback loop that is introduced forces the output of the system to be equal to the one of the gyroscope at lower frequencies, before the low pass filter's cutoff frequency.

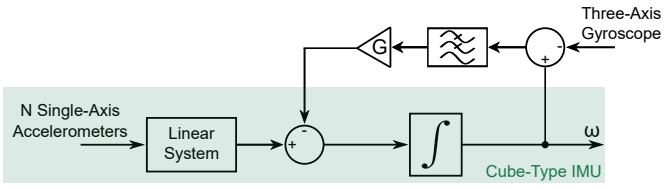

(a) Top-level architecture of the proposed system.

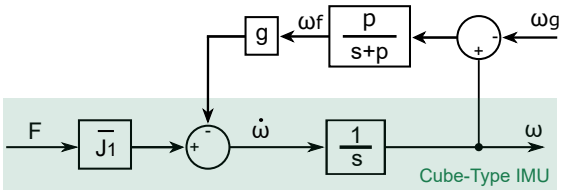

(b) Block diagram representation of the proposed system.

Fig. 2: Top level architecture (a) and block diagram representation (b) of the proposed system.

At higher frequencies, the feedback signal is attenuated and the systems output is dominated by the accelerometers' measurements.

Before continuing with the analysis of the system and since both the inputs (F and ω_g) and the output (ω) of the system are vectors, it is useful to define the following diagonal matrices related to the modeling of the feedback loop.

$$\begin{aligned} G &= \text{diag}(\begin{bmatrix} g & g & g \end{bmatrix}) \\ P &= \text{diag}(\begin{bmatrix} p & p & p \end{bmatrix}) \\ P_s &= \text{diag}(\begin{bmatrix} \frac{p}{s+p} & \frac{p}{s+p} & \frac{p}{s+p} \end{bmatrix}) \end{aligned} \tag{12}$$

Assume that the input measurements of both the accelerometer (F in Figure 2b) and the gyroscope (ω_g in Figure 2b) are not ideal and it is

$$F = F_i + \delta F \text{ and } \omega_g = \omega_{gi} + \delta\omega_g \tag{13}$$

where $F_i \in \mathbb{R}^6$ and $\omega_{gi} \in \mathbb{R}^3 \triangleq \omega$ are the ideal measurements of the the accelerometers and the gyroscope respectively and $\delta F \in \mathbb{R}^6$ and $\delta\omega_g \in \mathbb{R}^3$ represent the measurement error of the two sensors. Using this assumption and following the block diagram of Figure 2b, we write

$$\dot{\tilde{\omega}} = \bar{J}_1(F_i + \delta F) - G\omega_f \tag{14}$$

where

$$\bar{J}_1 = \frac{1}{2l^2} J_1. \tag{15}$$

Subtracting (9) from (14), we get the evolution of the system's output error in time

$$\dot{\delta\omega} = \bar{J}_1 \delta F - G\omega_f \tag{16}$$

Following Figure 2b, the feedback signal is written as

$$\begin{aligned} \omega_f &= P_s(\tilde{\omega} - \omega_{gi} - \delta\omega_g) \\ &= P_s(\delta\omega - \delta\omega_g) \end{aligned} \tag{17}$$

and its time derivative is derived as

$$\dot{\omega_f} = -P\ \omega_f + P(\delta\omega - \delta\omega_g) \tag{18}$$

Using (16) and (18), we write the following state-space system representation

$$\underbrace{\begin{bmatrix} \dot{\delta\omega} \\ \dot{\omega_f} \end{bmatrix}}_{\dot{x}} = \underbrace{\begin{bmatrix} 0_{3\times3} & -G \\ P & -P \end{bmatrix}}_{A} \underbrace{\begin{bmatrix} \delta\omega \\ \omega_f \end{bmatrix}}_{x} + \underbrace{\begin{bmatrix} \bar{J}_1 & 0_{3\times3} \\ 0_{3\times6} & -P \end{bmatrix}}_{B} \underbrace{\begin{bmatrix} \delta F \\ \delta\omega_g \end{bmatrix}}_{u} \tag{19}$$

The characteristic polynomial of A is

$$p_A(\lambda) = (\lambda^2 + p\lambda + gp)^3 \tag{20}$$

and its roots (which are the eigenvalues of A) are always negative for positive values of g and p. Thus A is always Hurwitz and the system of (19) is BIBO stable. This is an important result as it indicates that the output error of the proposed system, $\delta\omega$, is bounded for bounded inputs of the accelerometers' and the gyroscope's biases, δF and $\delta\omega_g$ respectively.

To quantify the effect of the accelerometers' and the gyroscope's biases on the system's output error, we assume a small constant bias vector $\bar{f} \in \mathbb{R}^6$ for the accelerometers and a small constant bias vector $\bar{\omega} \in \mathbb{R}^3$ for the gyroscope. From (19) we get

$$\begin{aligned} x(t) &= e^{At}x(0) + \int_0^t e^{A(t-s)} B \begin{bmatrix} \bar{f} \\ \bar{\omega} \end{bmatrix} \text{ds} \\ &= e^{At}x(0) + (e^{At} - I_6)A^{-1}B \begin{bmatrix} \bar{f} \\ \bar{\omega} \end{bmatrix} \end{aligned} \tag{21}$$

where I_6 is the 6×6 identity matrix. The steady state response of (19) is derived as

$$\begin{aligned} \lim_{t\to+\infty} x_(t) &= -A^{-1}B \begin{bmatrix} \bar{f} \\ \bar{\omega} \end{bmatrix} \\ &= \begin{bmatrix} \frac{\bar{J}_1\bar{f}}{g} + \bar{\omega} \\ \frac{\bar{f}}{g} \end{bmatrix} \end{aligned} \tag{22}$$

Using the triangle inequality and (22), we get the worst case scenario for the steady state value of $\delta\omega$ which is

$$\|\delta\omega\| \leq \left\| \frac{\bar{J}_1\bar{f}}{g} \right\| + \|\bar{\omega}\| \tag{23}$$

B. Noise Performance

To evaluate the noise performance of the proposed architecture, we performed simulations in MATLAB. More specifically, we excited both the accelerometers' and the gyroscope's inputs of the system of Figure 2b with band-limited white noise the characteristics of which were chosen to match the ones of a popular IMU in chip form [20]. The feedback's gain was set to $g = 20$ while the cut-off frequency of the low-pass filter was set to $p = 2\pi 0.2$ rad (0.2 Hz).

The power spectral density (PSD) of the system's output is presented in Figure 3 and compared to the PSD of the gyroscope's noise for two different values of the parameter l in Figure 1 which determines the distance between the accelerometers. As seen in in Figure 3, while the distance between the accelerometers gets longer, the output noise of the proposed system gets significantly lower in the higher frequencies (up to 30dB lower than the one of the gyroscope) where

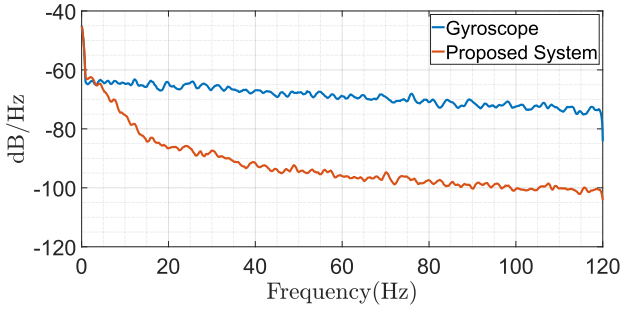

(a) $l = 0.5m$

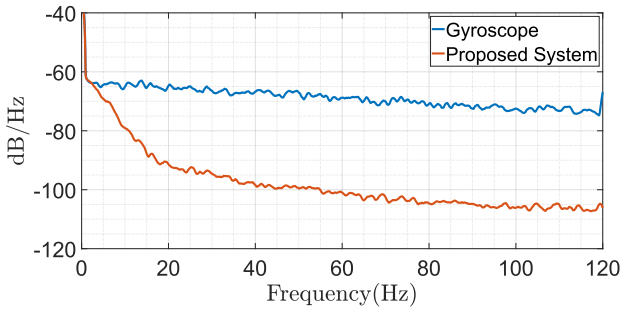

(b) $l = 2m$

Fig. 3: The PSD of the proposed system's output noise (X-axis) compared to the PSD of the gyroscope's output noise (X-axis) for $l = 0.5m$ (a) and $l = 2m$ (b).

the output is dominated by the accelerometers' measurements.

IV. Conclusion

In this work we introduced a new IMU architecture which expands a big class of existing systems and make them robust for use in real-world conditions. We demonstrated how existing works cannot be used with real sensors' data as they cannot compensate for the accelerometers' bias. Then, we analytically proved the ability of the proposed system to compensate for the accelerometers' bias. Furthermore we compared the output noise of the proposed system to the one of a gyroscope of the same grade. We demonstrated that when the accelerometers are spread over a great distance, the output noise of the proposed system is up to 30dB lower than the one of the gyroscope.

Acknowledgment

This research is co-financed by Greece and the European Union (European Social Fund- ESF) through the Operational Programme "Human Resources Development, Education and Lifelong Learning" in the context of the project "Strengthening Human Resources Research Potential via Doctorate Research" (MIS-5000432), implemented by the State Scholarships Foundation (IKY).

References

[1] P. D. Groves, *Principles of GNSS, Inertial, and Multisensor Integrated Navigation Systems*. Artech House, 2013.

[2] K. Papafotis and P. P. Sotiriadis, "Mag.i.c.al.–a unified methodology for magnetic and inertial sensors calibration and alignment," *IEEE Sensors Journal*, vol. 19, no. 18, pp. 8241–8251, Sep. 2019.

[3] J. F. Vasconcelos, G. Elkaim, C. Silvestre, P. Oliveira, and B. Cardeira, "Geometric approach to strapdown magnetometer calibration in sensor frame," *IEEE Transactions on Aerospace and Electronic Systems*, vol. 47, no. 2, pp. 1293–1306, April 2011.

[4] K. Papafotis and P. P. Sotiriadis, "Exploring the importance of sensors' calibration in inertial navigation systems," in *2020 IEEE International Symposium on Circuits and Systems (ISCAS)*, 2020, pp. 1–4.

[5] A. Noureldin, T. B. Karamat, and J. Georgy, *Fundamentals of Inertial Navigation, Satellite-based Positioning and their Integration*. Springer-Verlag Berlin Heidelberg, 2013.

[6] P. Groves, G. Pulford, C. Littlefield, D. Nash, and C. Mather, "Inertial navigation versus pedestrian dead reckoning: Optimizing the integration," vol. 2, 09 2007.

[7] J.-H. Chen, S.-C. Lee, and D. B. DeBra, "Gyroscope free strapdown inertial measurement unit by six linear accelerometers," *Journal of Guidance, Control, and Dynamics*, vol. 17, no. 2, pp. 286–290, 1994. [Online]. Available: https://doi.org/10.2514/3.21195

[8] F. Qin, J. Xu, and J. Sai, "A new scheme of gyroscope free inertial navigation system using 9 accelerometers," in *2009 International Workshop on Intelligent Systems and Applications*, 2009, pp. 1–4.

[9] J. Genin, J. Hong, and W. Xu, "Accelerometer placement for angular velocity determination," *Journal of Dynamic Systems, Measurement, and Control*, vol. 119, no. 3, pp. 474–477, Sep 1997. [Online]. Available: https://doi.org/10.1115/1.2801281

[10] A. J. Padgaonkar, K. W. Krieger, and A. I. King, "Measurement of angular acceleration of a rigid body using linear accelerometers," *Journal of Applied Mechanics*, vol. 42, no. 3, pp. 552–556, Sep 1975. [Online]. Available: https://doi.org/10.1115/1.3423640

[11] A. Li, F. Qin, J. Xu, and SaiJiang, "Gyroscope free strapdown inertial navigation system using rotation modulation," in *2009 Second International Conference on Intelligent Computation Technology and Automation*, vol. 3, 2009, pp. 611–614.

[12] F.-J. Qin, J.-N. Xu, and A. Li, "A novel attitude algorithm for 12 accelerometer based gfins using hermite interpolation," in *2010 International Conference on Measuring Technology and Mechatronics Automation*, vol. 1, 2010, pp. 214–217.

[13] E. Edwan, S. Knedlik, and O. Loffeld, "Constrained angular motion estimation in a gyro-free imu," *IEEE Transactions on Aerospace and Electronic Systems*, vol. 47, no. 1, pp. 596–610, 2011.

[14] S. Park, C.-W. Tan, and J. Park, "A scheme for improving the performance of a gyroscope-free inertial measurement unit," *Sensors and Actuators A: Physical*, vol. 121, no. 2, pp. 410–420, 2005. [Online]. Available: https://www.sciencedirect.com/science/article/pii/S0924424705001366

[15] C.-W. Tan and S. Park, "Design and error analysis of accelerometer-based inertial navigation systems," *Institute of Transportation Studies, UC Berkeley, Institute of Transportation Studies, Research Reports, Working Papers, Proceedings*, 01 2002.

[16] C.-W. Tan, K. Mostov, and P. Varaiya, "Feasibility of a gyroscope-free inertial navigation system for tracking rigid body motion," *Institute of Transportation Studies, UC Berkeley, Institute of Transportation Studies, Research Reports, Working Papers, Proceedings*, 01 2000.

[17] C.-W. Tan, S. Park, K. Mostov, and P. Varaiya, "Design of gyroscope-free navigation systems," in *ITSC 2001. 2001 IEEE Intelligent Transportation Systems. Proceedings (Cat. No.01TH8585)*, 2001, pp. 286–291.

[18] S. Park and C.-W. Tan, "Gps-aided gyroscope-free inertial navigation systems," *Institute of Transportation Studies, UC Berkeley, Institute of Transportation Studies, Research Reports, Working Papers, Proceedings*, 01 2002.

[19] E. Akeila, Z. Salcic, and A. Swain, "Implementation, calibration and testing of gfins models based on six-accelerometer cube," in *TENCON 2008 - 2008 IEEE Region 10 Conference*, Nov 2008, pp. 1–6.

[20] *BNO055 - Intelligent 9-axis absolute orientation sensor*, Bosch Sensortec, bst-bno055-ds000-14.